Available online at www.sciencedirect.com
ScienceDirect
Acta Materialia 55 (2007) 321–327
Acta MATERIALIA
www.actamat-journals.com

Deformation in a $Zr_{57}Ti_5Cu_{20}Ni_8Al_{10}$ bulk metallic glass during nanoindentation

Fuqian Yang [a,*], Kebin Geng [a], Peter K. Liaw [b], Guojiang Fan [b], Hahn Choo [b]

[a] Department of Chemical and Materials Engineering, University of Kentucky, Lexington, KY 40506, USA
[b] Department of Materials Science and Engineering, University of Tennessee, Knoxville, TN 37994, USA

Received 4 January 2006; received in revised form 29 June 2006; accepted 30 June 2006
Available online 24 October 2006

Abstract

Nanoindentation experiments of a $Zr_{57}Ti_5Cu_{20}Ni_8Al_{10}$ bulk metallic glass were performed with indentation loads ranging from 200 to 2000 μN. Both the indentation hardness and the reduced contact modulus decreased with the increase in the indentation load due to the propagation of shear bands underneath the indenter – the occurrence of a softening effect. The ratio of the indentation hardness to the reduced contact stiffness was a function of the reciprocal of the indentation depth. Based on the concept of diffusion-induced stresses, a one-dimensional constitutive relation between the change of the excessive free volume and the flow stress was proposed. The indentation-size effect as observed in the indentation tests was explained through the consideration of the contribution of the strain gradient in the constitutive relation.

Keywords: Metallic glass; Nanoindentation; Shear bands

1. Introduction

Bulk metallic glasses (BMGs) have a unique combination of mechanical properties [1–5], such as high modulus, hardness, elastic limit and strength, which has made them of great potential technological and scientific interest since their discovery in 1960 [6]. The flow in metallic glasses in general is inhomogeneous at high stresses and low temperatures, and is accommodated through the initiation and propagation of shear bands [7]. The occurrence of a serrated flow and the formation of shear bands underneath indents have been reported during the indentation test [8–14]. Donovan [12] observed the radial incipient cracks and the curving Hartmann lines in the deformation zone for the indentation of a $Pd_{40}Ni_{40}P_{20}$ metallic glass. Jana et al. [14] revealed several sets of slip-steps from shear bands for the Vickers indentation of $Pd_{42.1}Ni_{39.77}P_{18.13}$ and $Zr_{56.69}Cu_{26.96}Al_{10.95}Ni_{5.4}$. Zhang et al. [8] investigated the evolution of shear bands in Vitreloy 106 beneath a Vickers indentation and suggested that, at small indentation loads, the material flow was primarily accommodated by semi-circular primary shear bands surrounding the indentation. There have been few reports on the observation of shear bands over the contact surface, which are likely smoothened by the indenter surface, as suggested by Zhang et al. [8].

The occurrence of a serrated flow was reported by Wang et al. [15] in the indentation of a Zr-based metallic glass, which might be associated with the discrete pop-in phenomenon. Golovin et al. [16] observed the occurrence of the pop-in in the loading phase for the indentation of a Pd-based BMG and noted the dependence of the strain-serrations on the indentation depth. They claimed that the hardness and Young's modulus are nearly independent of the indentation rate, while Schuh et al. [17] suggested the dependence of the plastic flow on the indentation rate. Recently, Greer et al. [18] indicated that the absence of a serrated flow and the pop-in phenomenon

* Corresponding author.
E-mail address: fyang0@engr.uky.edu (F. Yang).

1359-6454/$30.00
doi:10.1016/j.actamat.2006.06.063

at low indentation depths may be due to the lack of resolution in the instrument.

To date, most work in nanoindentation has focused on the characterization of the hardness and Young's modulus, and the observation of a serrated flow. Few studies have paid attention to the evaluation of the energy dissipated in each indentation and the effect of the indentation load on the dissipation of energy. In this work, we characterize the indentation deformation of a $Zr_{57}Ti_5Cu_{20}Ni_8Al_{10}$ BMG under different indentation conditions. The indentation hardness is studied in order to assess the effect of the indentation load and to determine the inhomogeneous deformation. The dependence of the energy dissipated in the indentation on the indentation load is also discussed.

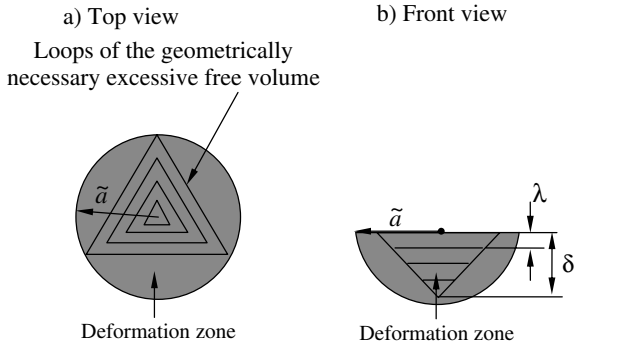

Fig. 1. Schematic of the equally distributed loops of the geometrically necessary excessive free volume under the indentation: (a) top view and (b) front view.

2. Analysis of the indentation deformation

It is known that the excessive free volume coalesces in metallic glasses during plastic flow. This trend changes atomic orders and likely creates local stresses. Extending the concept of diffusion-induced stresses [19–21] and considering the second-order kinetics for the annihilation of the excessive free volume [22], one can express the one-dimensional relation between the flow stress and the change of the excessive free volume induced by the nucleation and formation of the excessive free volume as

$$\sigma = \alpha K \Omega \sqrt{\Delta V} \tag{1}$$

where σ is the uniaxial flow stress, K is the bulk modulus, Ω is the volume of each free volume unit, V is the concentration of the excessive free volume and α is a constant associated with the Helmholtz free energy and temperature for the stress-assisted nucleation and formation of the excessive free volume. In general, the strain gradient plays an important role in determining the deformation behavior of materials in nanoindentation at the nano- to submicrometer scales. It is expected that the excessive free volume underneath the indenter consists of the statistically excessive free volume and geometrically necessary excessive free volume induced by the strain gradient. Thus, one can rewrite Eq. (1) as

$$\sigma = \alpha K \Omega \sqrt{\Delta V_S + \Delta V_G} \tag{2}$$

where V_S and V_G are the concentration of the statistically – stored excessive free volume and geometrically – necessary excessive free volume, respectively. For the nanoindentation of a BMG by a Berkovich indenter, the indentation deformation is accompanied by the formation and growth of equally distributed loops of the geometrically necessary excessive free volume [23], as shown in Fig. 1. One can approximate the geometrical configuration of the loops as equilateral triangles, since the Berkovich indenter is a three-sided pyramid. The length of the first triangular loop, L_1, near the free surface is

$$L_1 = 3\sqrt{3}\tilde{a} \tag{3}$$

Here $\tilde{a}$ is the radius of the deformation zone underneath the indenter. Using the principle of the geometrical similarity, one obtains

$$\begin{aligned} L_2 &= \frac{\delta-\lambda}{\delta}L_1, \quad L_3 = \frac{\delta-2\lambda}{\delta-\lambda}L_2 = \frac{\delta-2\lambda}{\delta}L_1, \ldots, L_n \\ &= \frac{\delta-(n-1)\lambda}{\delta-(n-2)\lambda}L_{n-1} = \frac{\delta-(n-1)\lambda}{\delta}L_1 \end{aligned} \tag{4}$$

where δ is the indentation depth, λ is the characteristic spacing between the triangular loops of the geometrically necessary excessive free volume and $n = \lfloor \delta/\lambda \rfloor$ (the greatest integer less than or equal to δ/λ). Thus, the total length of the triangular loops, L, as a function of the indentation depth, δ, can be calculated as

$$L = \sum_1^n L_n = L_1\left[n - \frac{\lambda}{\delta}\frac{n(n-1)}{2}\right] \tag{5}$$

Approximating $n \approx \delta/\lambda$ and assuming $\delta/\lambda \gg 1$, one can simplify Eq. (5) as

$$L = \frac{3\sqrt{3}\tilde{a}\delta}{2\lambda} \tag{6}$$

With the geometrically necessary excessive free volume accumulating in the deformation zone, the change in the concentration of the geometrically necessary excess free volume associated with the indentation deformation is

$$\Delta V_G = \frac{9\sqrt{3}\tan^2\theta}{16\pi\lambda\delta} \tag{7}$$

where θ is the angle between the surface of the material and the side surface of the indenter. As pointed out by Schuh and Nieh [13], the indentation hardness for a metallic glass can be related to the uniaxial flow stress as

$$H = \chi\sigma \tag{8}$$

where χ in general is a function of the surface profile of the indenter and the mechanical properties of the material. The value of $\chi \sim 3$ is a good approximation for metallic glasses [13]. Substitution of Eqs. (7) and (8) into Eq. (2) yields

$$H = \alpha\chi\Omega K\sqrt{\Delta V_S + \frac{9\sqrt{3}\tan^2\theta}{16\pi\lambda\delta}} \quad (9)$$

Using the relationship between the bulk modulus and Young's modulus, one can rewrite Eq. (9) as

$$\frac{H}{E} = \frac{\alpha\chi\Omega\sqrt{\Delta V_S}}{3(1-2\nu)}\sqrt{1+\frac{\delta_0}{\delta}} \quad (10)$$

Here E and ν are Young's modulus and Poisson's ratio of the material, respectively, and δ_0 is defined as

$$\delta_0 = \frac{9\sqrt{3}\tan^2\theta}{16\pi\lambda\Delta V_S} \quad (11)$$

The indentation hardness of metallic glasses is a function of the reciprocal of the indentation depth and displays the size effect. For a larger indentation depth with $\delta \gg \delta_0$, the second term on the right-side of Eq. (10) is negligible, and the indentation hardness is proportional to the Young's modulus as expected.

3. Experimental

A BMG with the composition of $Zr_{57}Ti_5Cu_{20}Ni_8Al_{10}$ at.% was used in the experiments. The ingots of master alloy were prepared by arc-melting mixtures of pure Zr, Ti, Cu, Ni and Al metals in a Ti-gettered high purity argon atmosphere. A special Zr crystal rod (<0.05 at.% oxygen) was used in order to maintain the low-oxygen concentration of the alloys [24]. The ingot alloys were remelted at temperature of 1200 K several times to ensure homogeneity. The cast rod, 5 mm in diameter and 60 mm in length, was made at a cooling rate of 100 K/s, using a suction-casting method in an arc furnace via a pseudo-floating-melt state before casting to obtain a completely melted state [24]. The samples were machined into a disk shape with a diameter of 5 mm and thickness of 1.5 mm. The samples were then ground and polished mechanically to obtain two parallel surfaces of mirror quality to avoid surface effects. X-ray diffraction (XRD) analyses were performed on the samples to characterize the structure.

The nanoindentation tests were performed in a Hysitron TriboScope (Minneapolis, MN) mounted on a Quesant atomic force microscope (AFM) (Agoura Hills, CA). The diamond tip was used with a pyramid-shaped Berkovich indenter of 70 nm in radius. Constant loading and unloading rates were used in the indentation tests. The penetration depth and applied load were used in the characterization of the near-surface mechanical behavior of the $Zr_{57}Ti_5Cu_{20}Ni_8Al_{10}$ BMG.

4. Results and discussion

The XRD was conducted to confirm the glass structure of the $Zr_{57}Ti_5Cu_{20}Ni_8Al_{10}$ BMG. The result of the XRD is presented in Fig. 2. There is only a broad diffraction peak,

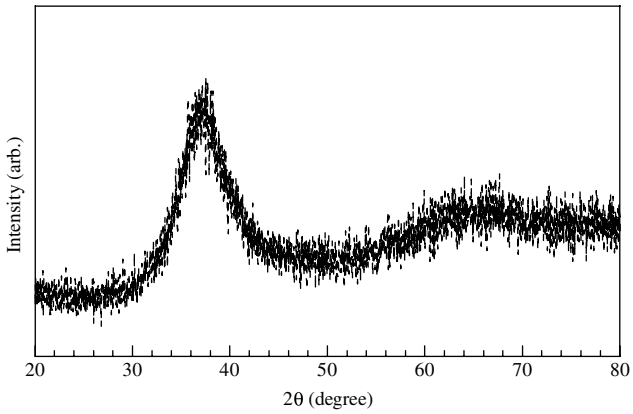

Fig. 2. XRD patterns of the as-cast $Zr_{57}Ti_5Cu_{20}Ni_8Al_{10}$ BMG.

which corresponds to an amorphous structure. No peaks associated with any crystalline phase can be observed.

The nanoindentation tests were carried out using the load-control mode with the indentation load in the range 200–2000 μN and zero holding time at the peak indentation load. Constant loading and unloading rates were used with the loading and unloading times both of 10 s, corresponding to loading/unloading rates of 20–200 μN/s. AFM was used to image selected impression marks. For the experimental conditions used in the work, no serrated flow during the loading and unloading and multiple circular shear-steps outside the impression marks were observed. Fig. 3 shows a typical AFM image of the impression mark indented at an indentation load of 1500 μN and the corresponding morphological profiles of the residual indentation. The indentation profiles are self-similar, and a pile-up around the indentation can be observed. The highest pile-up occurs at the region closest to the contact surface, A, where the surface became wrinkled due to greater inhomogeneity of the flow.

For homogeneous materials, the relationship between the indentation load and the maximum indentation depth can be described by the following equation [25,26]:

$$F = K_m\delta^n \quad (12)$$

where K_m is a constant related to the deformation behavior of the material and n is an exponential index. Fig. 4 shows the dependence of the maximum indentation depth on the maximum indentation load with a zero holding time, in which the results were averaged over more than five indentations for each testing condition. One obtains an exponential index of 1.1, which is different from the value of 2 obtained using dimensional analysis for a geometrically similar indenter [27]. It has been reported that metallic glasses do not obey either the Tresca or von-Mises yield criterion [13]. Instead, metallic glasses exhibit some pressure or normal-stress dependence to the yield criterion, such as the Mohr–Coulomb criterion and the Drucker–Prager yield criterion. This trend limits the use of the von-Mises flow rule in the analysis of the deformation behavior of BMG materials and suggests that the dimensional analysis

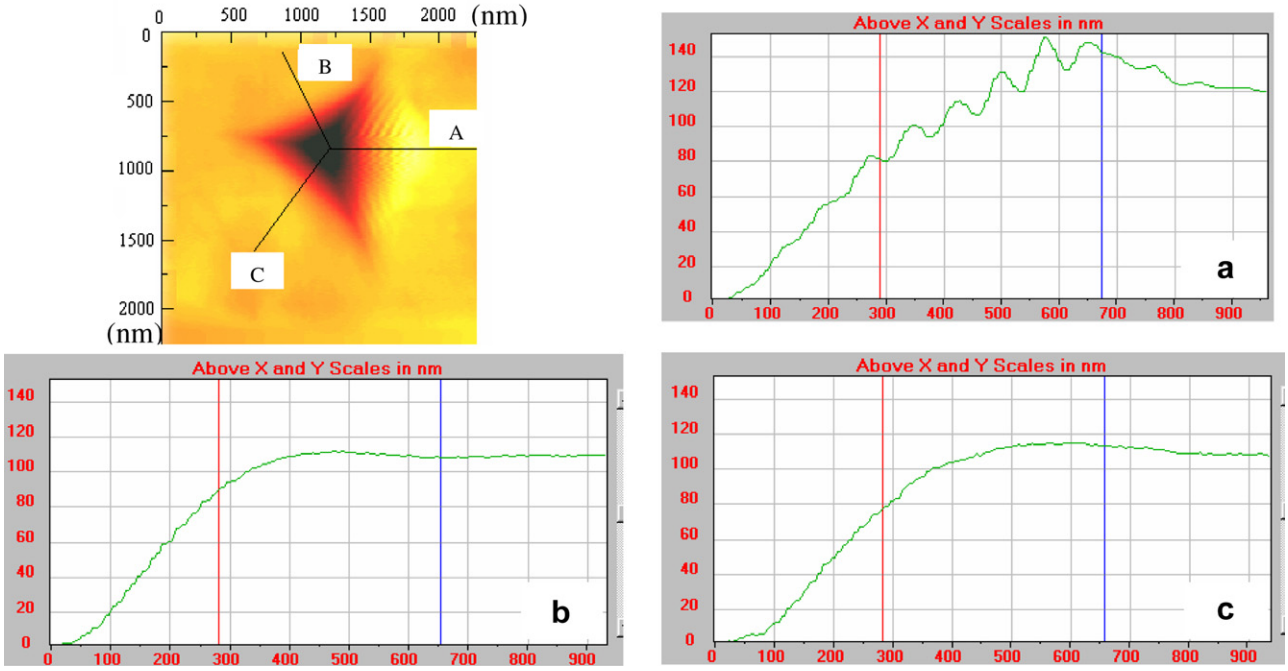

Fig. 3. Slip-step patterns from the propagation of shear bands over the contact surface and the surrounding area.

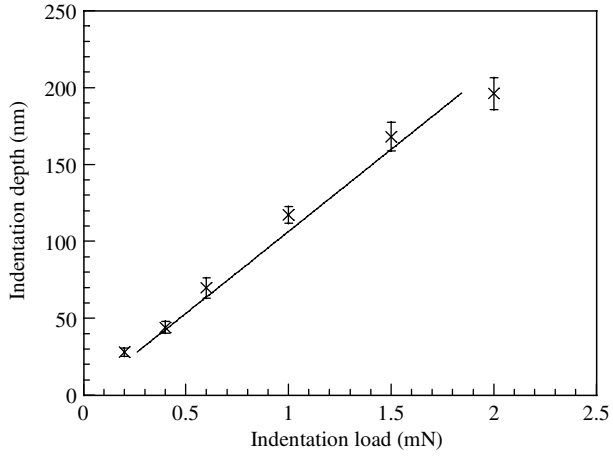

Fig. 4. Dependence of the maximum indentation depth on the indentation load with a zero holding time.

based on the von-Mises flow rule is probably inapplicable for the description of the indentation deformation in BMG materials. Thus, the exponential index in Eq. (12) may be different from the value of 2 obtained from the dimensional analysis [28].

In the analysis of the indentation deformation, we simply use the O–P approach [29] without considering the effect of the material pile-up due to the difficulty in accurately measuring the size of the pile-up at the submicrometer scale. Also, no bulge behavior is observed during the unloading, which suggests that there is no significant viscoelastic deformation under the indentation conditions. From the loading–unloading curves, one can calculate the reduced contact modulus of the $Zr_{57}Ti_5Cu_{20}Ni_8Al_{10}$ BMG from the upper portion of the unloading curves. The dependence of the reduced contact modulus, E_r, on the indentation load with a zero-holding time is depicted in Fig. 5. The reduced contact modulus decreases with the indentation load. The basic mechanism for this phenomenon is not well understood at this moment, but will be studied in the future. Compared with simple tensile and compressive tests, a complicated stress field in materials is created due to the contact between two solid surfaces. The excessive free volume as generated during the indentation coalesces in the shear bands and leads to nucleation and formation of voids. In the region subjected to the tensile stress, growth and linkage of voids are facilitated, which causes less dense packing of atoms with a larger average interatomic spacing. This trend weakens the

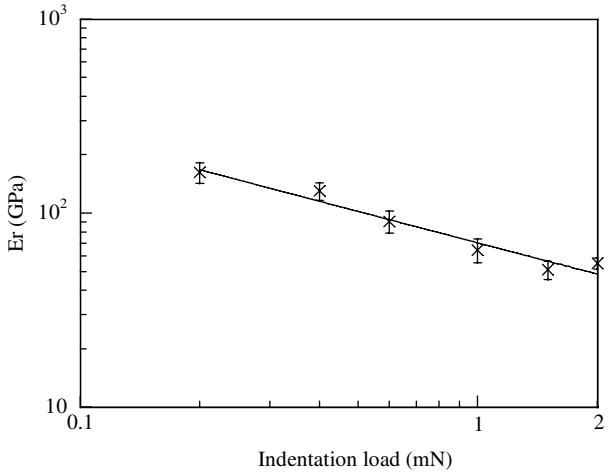

Fig. 5. Effect of the indentation load on the reduced contact stiffness.

mechanical strength of the material and causes a reduction in the local elastic modulus. In the deformation zone subjected to a compressive stress, the growth of voids is retarded. The overall effect of the stress-assisted formation of the excessive free volume and the nucleation and formation of voids results in a reduction of the nominal elastic modulus underneath the indentation and a decrease of the reduced contact stiffness with the indentation load.

The dependence of the indentation hardness on the indentation load is depicted in Fig. 6. Similar to the indentation size effect observed in crystalline and polymeric materials, the indentation hardness decreases with the increase of the indentation load. In general, the amount of the excessive free volume as generated during the indentation increases with an increase in the indentation load, and the plastic deformation zone increases with the indentation load. Even though more excessive free volume is nucleated during the indentation, the specific growth rate of the plastic zone is higher than the specific nucleation rate of excessive free volume. This leads to a decrease in the average concentration of the excessive free volume.

The ratio of the indentation hardness to the reduced contact modulus is shown in Fig. 7 as a function of the reciprocal of the indentation depth. Considering that the contribution of the system stiffness to the reduced contact stiffness is negligible, one can assume that Young's modulus of the metallic glass is proportional to the reduced contact modulus. Using the reduced contact modulus in Eq. (10), a straight line is fitted through the data points, which supports the proposed model. This suggests that the strain gradient contributes to the nucleation and formation of the excessive free volume for the indentation on the nano- and submicrometer scales and confirms the dependence of the stresses on the variation of the excessive free volume as described by Eq. (2).

Another way of evaluating the indentation behavior of materials is by analyzing the dependence of the parameter F/S^2 on the indentation load, as suggested by Joslin and Oliver [30]. Here S is the contact stiffness. Using the definition of the indentation hardness and the solution given by Sneddon [31], one can obtain [32]

$$\frac{F}{S^2} = \frac{\pi}{4\beta^2}\frac{H}{E_r^2} \tag{13}$$

where β is a constant depending on the geometry of the indenter. The ratio of F/S^2 is proportional to the indentation hardness and inversely proportional to the square of the reduced contact modulus. The dependence of the contact stiffness on the indentation load is depicted in Fig. 8, from which one concludes that the F/S^2 is a constant independent of the indentation load, suggesting that the ratio of H/E_r^2 be a constant independent of the indentation load. Fig. 9 shows the relationship between the indentation hardness and the reduced contact modulus. The indentation hardness is proportional to the square of the reduced contact modulus, which supports Eq. (13). This suggests that, for the metallic glass, the indentation-size effect for the indentation hardness is related to the decrease of the reduced contact stiffness with the increase in the indentation load. This confirms the observations in Figs. 5 and 7.

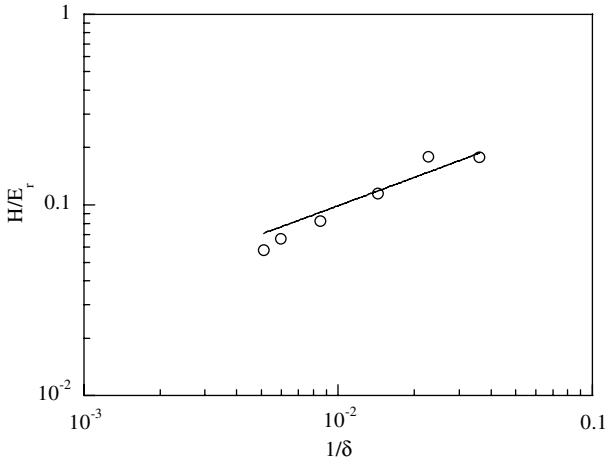

Fig. 7. Indentation-size effect in the indentation of a $Zr_{57}Ti_5Cu_{20}Ni_8Al_{10}$ BMG.

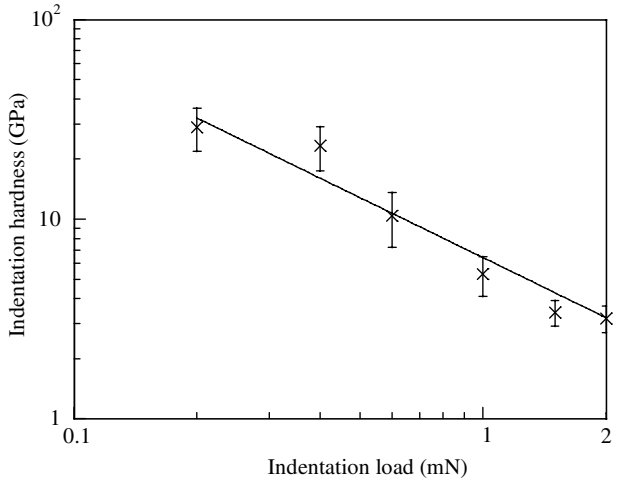

Fig. 6. Dependence of the indentation hardness on the indentation load.

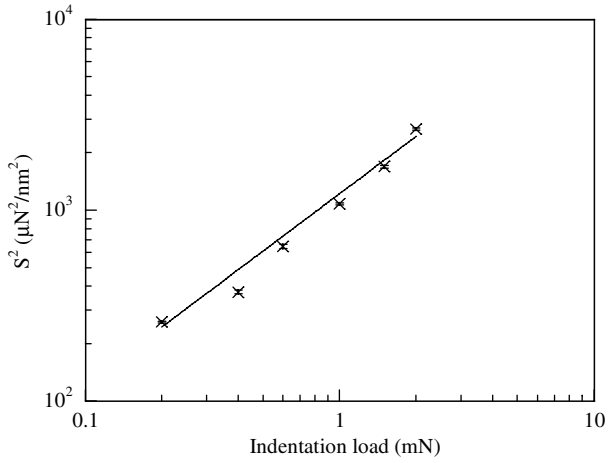

Fig. 8. Dependence of the contact stiffness on the indentation load.

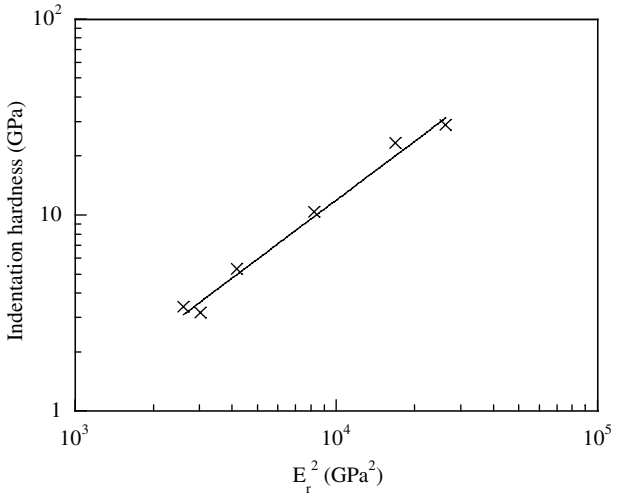

Fig. 9. Correlation between the indentation hardness and the reduced contact modulus.

The plastic energy dissipated, $E_{plastic}$, in an indentation loading–unloading cycle can be calculated from the area in the indentation load vs. indentation depth curve. The dissipated energy is a function of the indentation load and the mechanical properties of materials. Using the similarity analysis, Cheng et al. [28] found that the plastic energy dissipated in indentations using geometrically similar sharp indenters is proportional to the 3/2 power of the indentation load independent of the constitutive relationship of materials. Fig. 10 shows the dependence of the energy dissipated in the indentation on the indentation load. The dissipated energy increases with the increase of the indentation load, since more shear bands are created. A power-law relationship between the dissipated energy and the indentation load is used to fit the data points, as shown in Fig. 10. One obtains an index of 2.4, different from 3/2. This trend suggests that one needs to identify the fundamental mechanisms controlling the deformation behavior of metallic glasses, such as the nucleation and

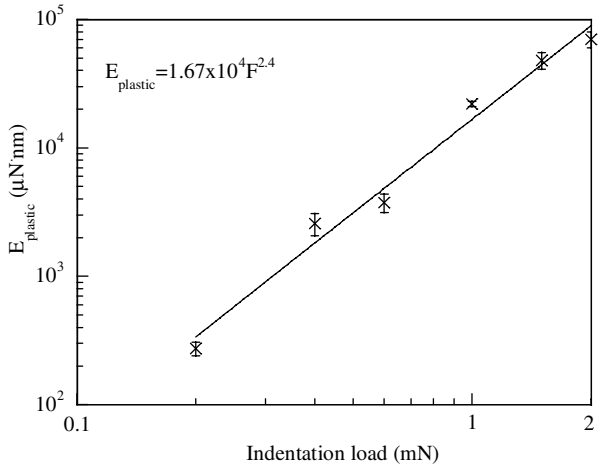

Fig. 10. Dependence of the energy dissipated in the indentation on the indentation load.

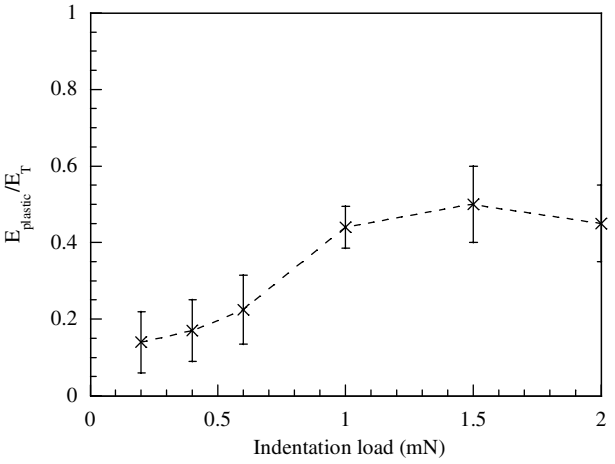

Fig. 11. Dependence of the energy ratio of $E_{plastic}/E_T$ on the indentation load.

propagation of the shear bands and the nanoindentation-induced nanocrystallization when subjected to high indentation load, and to incorporate the scaling effects and atomic migrations into the continuum mechanics for the description of the flow behavior of metallic glasses under the indentation.

Several studies [28,33–35] have tried to relate the ratio of the dissipated plastic energy to the total energy in the indentation to the mechanical properties of materials since Shorshorov [34] first related the dissipated plastic energy to the ratio of the hardness to the elastic modulus. Using similarity analysis and finite-element simulation, Cheng et al. [28] obtained a single one-to-one relationship for a conical indenter, independent of material properties and the geometry of the conical indenter. Using the indentation loading–unloading curves, the ratio of the dissipated plastic energy to the total energy in the indentation, $E_{plastic}/E_T$, is calculated and depicted in Fig. 11 as a function of the indentation load. In contrast to the analyses in the literature [28,34,35], the value of $E_{plastic}/E_T$ for the nanoindentation of the $Zr_{57}Ti_5Cu_{20}Ni_8Al_{10}$ BMG increases with the indentation load, reaching a constant value of about 0.45. At a small indentation load, there is not enough driving force for the nucleation of the excessive free volume and the formation of the shear bands underneath the indent. Fewer shear bands are formed, and the indentation deformation is controlled more by the elastic indentation. With the increase in indentation load, the rates (per unit force) for the nucleation of the excessive free volume and the formation of the shear bands increase, and more mechanical work is dissipated in the irreversible reactions. A further increase in the indentation load makes the rates approach constant value, and the ratio of $E_{plastic}/E_T$ becomes independent of the indentation load.

5. Conclusion

The flow behavior of metallic glasses is inhomogeneous and associated with the coalescence of the excessive free

volume and the formation of voids in the shear bands. Extending the concept of diffusion-induced stresses, we established a one-dimensional constitutive relation between the change of the excessive free volume and the flow stress. The indentation-size effect was revealed by considering the contribution of the strain gradient in the new constitutive relation.

The indentation deformation of a $Zr_{57}Ti_5Cu_{20}Ni_8Al_{10}$ BMG was characterized using the nanoindentation with indentation loads ranging from 200 to 2000 μN. The nanoindentation tests were performed in the load-control mode. No serrated flow was revealed from the loading–unloading curves. Both the indentation hardness and the contact modulus decreased with the increase in indentation load, which was due to the coalescence of the excessive free volume and the formation of voids in the shear bands during the indentation. An indentation-size effect was observed, which supported the proposed model. The plastic energy dissipated in the nanoindentation increased with the indentation load and was proportional to the 2.4 power index of the indentation load. The ratio of the dissipated plastic energy to the total energy in the indentations was found to be a function of the indentation load, suggesting the inhomogeneous flow underneath the indenter.

Acknowledgments

The authors are grateful to Professor W.D. Nix (Stanford University) for valuable discussions. F.Y. is grateful for support from the NSF grant CMS-0508989 and the support from General Motors Corporation. P.K.L. and G.F. are supported by the International Materials Institutes (IMI) program, DMR-0231320, with Dr C. Huber as the program director.

References

[1] Ravhchandran G, Molinari A. Acta Mater 2005;53:4087.
[2] Johnson WL. MRS Bull 1999;24:42.
[3] Greer AL. Science 1995;267:1947.
[4] Inoue A. Acta Mater 2000;48:279.
[5] Kim JJ, Choi Y, Suresh S, Argon AS. Science 2002;295:654.
[6] Duwez P, Wilens RH, Klement W. Appl Phys Lett 1960;31:1136.
[7] Wright WJ, Hufnagel TC, Nix WD. J Appl Phys 2003;93:1432.
[8] Zhang HW, Jing XN, Subhash G, Kecskes LJ, Dowding RJ. Acta Mater 2005;53:3849.
[9] Vaidynathan R, Dao M, Ravichandran G, Suresh S. Acta Mater 2001;49:3781.
[10] Conner RD, Li Y, Nix WD, Johnson WL. Acta Mater 2004;52:2429.
[11] Xing LQ, Li Y, Ramesh KT, Li J, Hufnagel TC. Phys Rev B 2001;64:180201.
[12] Donovan PE. J Mater Sci 1989;24:523.
[13] Schuh CA, Nieh TG. J Mater Res 2004;19:46.
[14] Jana S, Ramamurty U, Chattopadhyay K, Kawamura Y. Mater Sci Eng A 2004;375–377:1191.
[15] Wang JG, Choi BW, Nieh TG, Liu CT. J Mater Res 2000;15:798.
[16] Golovin YI, Ivogin VI, Khonik VA, Kitagawa K, Tyurin AI. Scripta Mater 2001;45:947.
[17] Schuh CA, Lund AC, Nieh TG. Acta Mater 2004;52:5879.
[18] Greer AL, Castellero A, Madge SV, Walker IT, Wilde JR. Mater Sci Eng A 2004;375–377:1182.
[19] Prussin S. J Appl Phys 1961;32:1876.
[20] Li JCM. Metall Trans A 1978;9A:1353.
[21] Yang FQ. Mater Sci Eng A 2005;409:153.
[22] Tuinstra P, Duine PA, Sietsma J, van den Beukel A. Acta Metall Mater 1995;43:2815.
[23] Lam DCC, Chong ACM. Mater Sci Eng A 2001;318:313.
[24] Wang GY, Liaw PK, Peter WH, Yang B, Yokoyama Y, Benson ML, et al. Intermetallics 2004;12:885.
[25] Yang FQ, Peng LL, Okazaki KJ. Metall Mater Trans A 2004;35:3323.
[26] Hay JL, Oliver WC, Bolshakv A, Pharr GM. Mater Res Soc Symp Proc 1998;522:101.
[27] Cheng YT, Cheng CM. Int J Solids Struct 1999;36:1231.
[28] Cheng YT, Li Z, Cheng CM. Philos Mag A 2002;82:1821.
[29] Oliver WC, Pharr GM. J Mater Res 1992;7:1564.
[30] Joslin DL, Oliver WC. J Mater Res 1990;5:123.
[31] Sneddon IN. Int J Eng Sci 1965;3:47.
[32] Saha R, Nix WD. Mater Sci Eng A 2001;319–321:898.
[33] Dao M, Chollacoop N, Van Vliet KJ, Venkatesh TA, Surech S. Acta Mater 2001;49:3899.
[34] Shorshorov MK, Bulychev SI, Alekin VP. Sov Phys Dokl 1981;26:769.
[35] Malzender J. J Mater Res 2004;19:1605.